Two-dimensional ultrafast infrared vibrational echo studies of solute–solvent interactions and dynamics

David E. Thompson, K. A. Merchant, and M. D. Fayer
Department of Chemistry, Stanford University, Stanford, California 94305

(Received 14 March 2001; accepted 9 April 2001)

Two-dimensional spectrally resolved ultrafast infrared vibrational echo experiments were used to investigate the nature of solute–solvent interactions in solution. The experiments were performed on (acetylacetonato)dicarbonylrhodium(I) in dibutylphthalate at 150 K. The 2D spectra display features that reflect the 0–1 and 1–2 transitions and the combination band transition of the symmetric (*S*) and antisymmetric (*A*) CO stretching modes. Three oscillations in the data arise from the frequency difference between the *S* and *A* modes (quantum beats) and the *S* and *A* anharmonicities. The novel mechanism that gives rise to the anharmonic oscillations, which is distinct from that of a conventional quantum beat, is described. The frequency of the *S*/*A* mode-splitting quantum beats varies for different observation wavelengths across the 0–1 inhomogeneous lines. For either the *S* or *A* lines, as the wavelength of observation of the vibrational echo is moved to higher energy, the quantum beat frequency decreases. The change in frequency is related to the nature of the solute–solvent interactions (inhomogeneous broadening) of the *S* and *A* transitions. A simple analytical approach is used to determine how a solute vibrational oscillator is influenced by the solvent. Three models of solute–solvent interactions are considered in terms of CO local mode energies and coupling. In one, the transition energies in the *S* and *A* lines are anticorrelated either because the inhomogeneous broadening arises from variations in the local mode coupling or the local mode energies are anticorrelated. In the other two, the local mode energies are either correlated or uncorrelated. The results of the model calculations indicate that interactions with the solvent result in local mode frequencies that are strongly correlated. © *2001 American Institute of Physics*. [DOI: 10.1063/1.1376423]

I. INTRODUCTION

One of the most important and fundamental questions in chemistry, biophysics, and materials science is how the internal mechanical degrees of freedom (vibrations) of a molecule or a portion of a macromolecule (e.g., a protein) are affected by their surroundings. When a solvent surrounds a molecule, its structure and dynamics change. In going from the gas phase to a condensed matter environment, vibrational energies change. The energy shifts are observable in infrared (IR) absorption spectra. Such shifts demonstrate that the structure of a molecule is influenced by interactions with a solvent, but the spectrum alone cannot, in general, be used to determine the nature of the solute–solvent interactions. Time dependent IR experiments, particularly optical coherence experiments, such as the ultrafast vibrational echo, can be used to investigate solute–solvent vibrational dynamics.[1–8] The vibrational echo technique has great utility in the investigation of solute–solvent intermolecular interactions, particularly when combined with detailed theoretical models[9] or simulations.[10] But, the one-dimensional vibrational echo has limits on the extent of the information it can provide. Methods are needed that can provide direct information on how the medium in which a molecule is embedded modifies its structural degrees of freedom. Are solvent interactions local or nonlocal? Do different parts of a molecule experience the same or different influences from the solvent? In this paper, ultrafast IR two-dimensional (2D) vibrational echo experiments are presented and used to address such questions.

In the 1970s, the extension of nuclear magnetic resonance (NMR) to 2D methods[11] vastly increased the usefulness of NMR in many areas of science. Recently, ultrafast 2D photon echo experiments on electronic excited states have been performed.[12,13] In the study of molecular matter, vibrational spectra are of particular importance because they reflect the mechanical structure of molecules. Here we present ultrafast infrared 2D (time-frequency) vibrational echo experiments that expand the types of information that can be obtained from vibrational spectroscopy.[14–16] The experiments are used to study intermolecular interactions and dynamics of (acetylacetonato)dicarbonylrhodium(I) ($Rh(CO)_2acac$) in a solid solution of dibutylphthalate.[14,17,18] $Rh(CO)_2acac$ has two ''local'' oscillators that provide a test bed for the investigation of the interactions of distinct parts of a molecule with a solvent. A solid glassy solvent provides an inhomogeneous environment that makes it possible to investigate how different local environments in a single solvent act on a molecule.

Ultrafast 2D vibrational echo methods combine the powerful experimental approaches used in NMR with the time resolution of ultrafast infrared pulses, permitting investigation of dynamics and interactions of the structural degrees of freedom of molecules in biological, chemical, and materials systems. Spectrally resolved ultrafast vibrational echo

spectroscopy[14] is an addition to an increasing collection of new 2D ultrafast IR spectroscopic methods.[5,6,19–24]

The experiments were conducted on the symmetric (S) and antisymmetric (A) CO stretching modes of $Rh(CO)_2$acac at $\sim$2000 cm^{-1}. The 2D vibrational echo spectrum (VES) is obtained by spectrally resolving the vibrational echo pulse with a monochromator. The 2D spectrum records the vibrational echo as a function of the detection frequency and the time delay (τ) between excitation pulses. The time structure on the vibrational echo pulse contains a substantial amount of information about the molecular oscillator/solvent system. Spectrally resolving the vibrational echo pulse Fourier transforms it from the time domain to the frequency domain, which reveals the time structure of the echo pulse through its frequency components.

The bandwidth of the ultrashort ($<$200 fs) IR pulses exceeds the anharmonicity of vibrational transitions and the frequency differences between the S and A vibrational modes, resulting in coherent excitation of multiple vibrational excited states. Vibrational echo decays are observed at the S and A, $v=0-1$ and $v=1-2$ transition frequencies as well as at transition frequencies involving the S/A combination band. These primary features are strongly modulated by two distinct types of oscillations. The longer period oscillations are caused by the anharmonicity of each mode.[2,23,25] It is shown below that these anharmonic oscillations are not a normal quantum beat,[14] and a new mechanism for the anharmonic oscillations is described. These oscillations are referred to as accidental degeneracy beats because they require inhomogeneous broadening and an accidental degeneracy between two different types of transitions that is made possible by the inhomogeneous broadening. The shorter period oscillations are conventional quantum beats arising from the splitting between the S and A peaks. In addition, the mechanism that gives rise to the combination band features in the spectrum, which involves simultaneous excitation of both the S and A transitions, is discussed. In linear spectroscopy, the combination band would appear in the spectrum at approximately the sum of the S and A transition frequencies, that is, $\sim$4000 cm^{-1}. However, in the vibrational echo spectrum, the combination band features are observed shifted from the S and A $v=0-1$ lines by the combination band shift (i.e., the difference between the combination band frequency and the sum of the A and S transition frequencies). By spectrally resolving the ultrafast vibrational echo and obtaining a 2D VES, the time resolution of the short pulses is preserved, the nature of the signal can be more readily elucidated, and additional information can be obtained.

In the results presented below, of particular importance is that analysis of the quantum beat data provides insights into the nature of solute–solvent interactions.[26] The frequency of the S/A quantum beats varies for different observation wavelengths across the $v=0-1$ inhomogeneous lines. Inhomogeneous broadening and its influence on the quantum beat frequency are discussed in terms of the CO local oscillator energies, their coupling to the solvent, and the coupling between the local oscillators that is responsible for the S and A modes. An analytical theory is employed. Three models of inhomogeneous broadening are considered in terms of the solvent induced spread in the CO local oscillator energies and the local oscillator coupling. In one, the transition energies in the S and A lines are anticorrelated either because the inhomogeneous broadening arises from variations in the local mode coupling or the local mode energies are anticorrelated. In the other two, the inhomogeneous distribution of local mode energies are either correlated or uncorrelated. Each model results in a distinct change in the beat frequency as the observation wavelength is changed. Analysis of the data indicates that the coupling of the two CO local oscillators to the solvent is highly correlated. A mechanism that could be responsible for the local oscillator correlation is proposed.

II. EXPERIMENTAL PROCEDURES

The 180 fs (FWHM) infrared pulses used in the experiments were generated at a 1 kHz repetition rate with a bandwidth (FWHM) of 90 cm^{-1}. The autocorrelation and the spectrum of the pulses are both close to Gaussian in shape. Their time-bandwidth product is 0.49, which is close to the transform limit of 0.44. The pulses were produced using a Spectra Physics optical parametric amplifier (BBO and $AgGaS_2$) pumped by a regeneratively amplified Ti:Sapphire system. The OPA was tuned to fix the center wavelength of the infrared pulses at $\sim$2045 cm^{-1}. This is approximately midway between the S (2082 cm^{-1}) and the A (2010 cm^{-1}) absorption bands. After leaving the OPA, a zinc selenide 15%–85% beam splitter was used to divide the infrared pulses into weaker pulses with wave vector k_1, and stronger pulses with wave vector k_2. A retro-reflector mounted on a computer controlled translation stage delayed the stronger pulses by a time τ relative to the weaker pulses. Traveling along parallel trajectories, separated by $\sim$1.25 cm, the well-collimated weak and strong pulses were directed into a 90° off axis parabolic reflector (PR). The PR focuses the beams and alters their direction of propagation so that they cross one focal length (15 cm) away from the PR. The $Rh(CO)_2$acac sample was centered at the crossing point of the two excitation beams.

The dibutylphthalate (DBP) and $Rh(CO)_2$acac used in preparing the sample were obtained from Aldrich. The DBP was distilled to eliminate dissolved water and the $Rh(CO)_2$acac was handled carefully in a glove box to minimize exposure to air. A $Rh(CO)_2$acac sample was contained in a 400 μm copper cell with CaF_2 windows. The cell was mounted on a continuous flow cryostat that cooled the sample to 150 K. Sample temperature was monitored with a silicon diode thermometer attached to one of the CaF_2 windows.

The vibrational echo signal, generated in the $2k_2-k_1$ direction, was spatially filtered with irises and then dispersed by a 210 line/mm grating in a 1 m monochromator. At the monochromator exit slit, a mercury cadmium telluride detector monitored the vibrational echo signal intensity. At each wavelength, a vibrational echo decay was collected as a function of τ using 34 fs steps near $\tau=0$ and 340 fs steps farther out. Between delay line scans, the monochromator was stepped 2 cm^{-1}. The combined data yield the A and S 2D vibrational echo spectra.

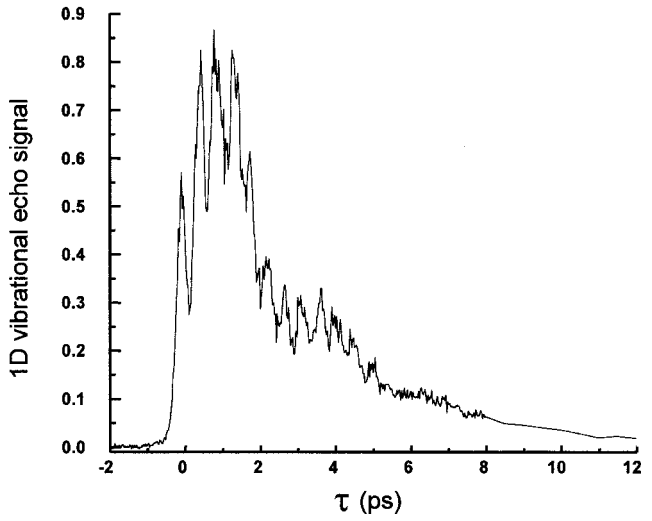

FIG. 1. The 1D vibrational echo decay of $Rh(CO)_2acac$ in dibutylphthalate at 150 K. The vibrational echo decay shows both high and low frequency oscillations.

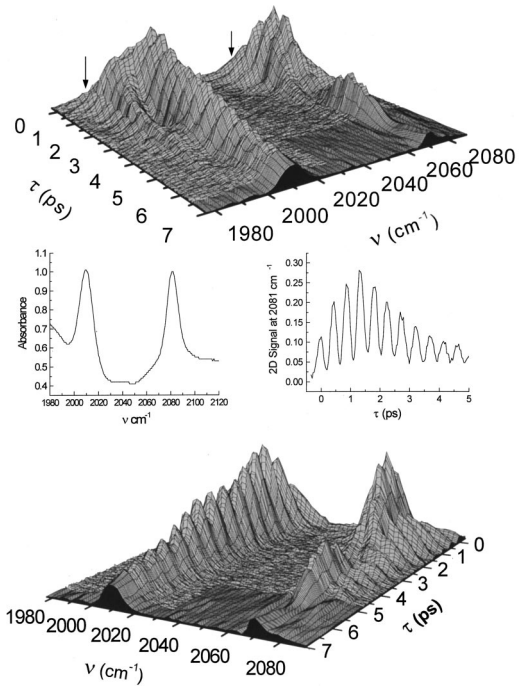

FIG. 2. The 2D vibrational echo spectrum of Rh(CO)2acac in dibutylphthalate at 150 K. The upper (lower) plot displays the VES spectrum from the red (blue) side. (Point spacing is 2 cm^{-1} on the frequency axis and 34 fs on the time axis. At long time, the spacing is 340 fs.) The 2D spectrum shows a dramatic increase in detail compared to the 1D decay shown in Fig. 1. The arrows highlight the echo signal arising from coherences involving the A/S combination band. The left inset is the room temperature absorption spectrum of the sample (solvent background is not subtracted). The right inset is a time slice of the 2D VES spectrum (the monochromator wavelength set at 2081 cm^{-1}) that shows the oscillations arising from quantum beating between the A and S modes.

III. RESULTS AND DISCUSSION

A. Features in the vibrational echo spectrum

Figure 1 displays a 1D vibrational echo decay, that is, τ is scanned and the total vibrational echo signal at all wavelengths is integrated. (The time resolution changes at 8 ps.) The signal is nonexponential and has oscillations at several frequencies. The data arise from a variety of multilevel coherences induced by the broadband excitation pulses. The signal has contributions from the $v=0-1$ and $v=1-2$ transitions of the S and A lines, as well as combination band transitions and quantum beats between the S and A lines. As discussed below, the quantum beats are not at a single frequency. The 1D data is sufficiently complex that interpretation is difficult. One approach to sorting out the various contributions to the data is to use narrow bandwidth IR pulses so that only a single transition is excited.[17,18] However, using a narrow bandwidth gives up the time resolution necessary to observe many of the features. In addition, information that can be obtained from, for example, the quantum beats, is not accessible because such information is only available when the bandwidth of the pulses is sufficient to produce multilevel coherences.

Rather than narrowing the bandwidth of the pulses, a better approach is to frequency resolve the vibrational echo pulse to yield a 2D vibrational echo spectrum. Figure 2 displays 2D vibrational echo spectra that span the full range of wavelengths of the S and A bands. The inset on the left shows the absorption spectrum. Note that the absorption spectrum has significant solvent features that are not present in the VES spectrum.[19,20] The solvent absorptions do, however, modify the VES spectrum by changing the interaction amplitude as a function of wavelength.[20,27] The S and A VES features are considerably broader than the corresponding linear absorption bands; the increase in breadth comes almost completely on the red side of the absorption center frequencies. The lower VES shows a rotated view of the A and S bands. The lower VES is shown from the blue side while the upper spectrum is shown from the red side. The inset on the right displays the time dependence at a single monochromator setting on the blue side of the S line at 2081 cm^{-1}.

Examining Fig. 2, a number of features are evident. First, the data has a high frequency modulation. The center portion of the A and S bands also display a much slower oscillation that is much less evident on the sides of each band. Examining the upper VES, it is clear that each band actually consists of three overlapping peaks. The various features will be discussed first, and then a detailed examination of the high frequency oscillations will be used to provide insights into the nature of solute–solvent interactions that are responsible for inhomogeneous broadening.

The S and A bands have contributions from the ground state ($v=0$) to first excited vibrational state ($v=1$) transition and from the $v=1$ state to the second vibrationally excited state ($v=2$, overtone) transition. The 0–1 contributions are on the blue side of each band. The 0–1 transitions correspond to the linear absorption peaks. Smaller features seen on the far red side of the bands (marked by arrows on the upper VES) are from combination band transitions discussed below. The features are only accessible because vibrational echoes are χ^3 processes involving three successive interactions of the sample with the incident radiation fields. (Phase matching constraints in the detection geometry prevent the $v=3$ level from participating in vibrational echo signal.)

The decay of the spectrum reflects the homogeneous dephasing of the system. The 0–1 transition (blue side of the line) decays somewhat more slowly than the 1–2 transition, and the combination band peak decays more quickly. This can been seen most clearly on the *A* peak of the upper VES. A complete determination of the pure dephasing linewidths will not be presented here. The decay of the 0–1 portions of the *A* and *S* bands are almost identical and yield a $T_2 = 16$ ps, which is in accord with previous measurements.[18] The homogeneous linewidths $(1/\pi T_2)$ are 2/3 cm^{-1} while the absorption linewidths are >10 cm^{-1} (see below), demonstrating that at the experimental temperature (150 K), the system is massively inhomogeneously broadened. The 1–2 portions of the decay are very similar to the 0–1 decays, but the combination band peaks appear to decay more rapidly. In a simple model that ignores fluctuations in the coupling between the two modes, the decay of the combination band peak would be closely related to the homogeneous dephasing of the *S* and *A* modes. The more rapid decays of the combination band peaks suggest that fluctuations of the anharmonic coupling may play a role in the combination band dephasing.

The central, overlapping portions of the 0–1 and 1–2 peaks exhibit low frequency oscillations. The oscillations are at the frequency of the anharmonic shift, that is, the difference between the 0–1 and 1–2 transition frequencies, 10.7 cm^{-1} for the *S* mode and 13.7 cm^{-1} for the *A* mode.[2,14,28] The lower frequency anharmonic oscillations are not quantum beats or other types of beats[14] seen in coherence experiments on a variety of multilevel systems.[29,30] The anharmonic oscillations are observed in spite of the fact that the vibrational echo is detected through a monochromator with a narrow band pass (2 cm^{-1}).[14] The origin of the oscillations is different from the one proposed previously for experiments without frequency resolution[2,31] and applies to experiments with and without spectral resolution.[14]

The anharmonic oscillations have their origin in two sets of Feynman diagrams describing single and double excitations of a vibrational mode, namely two-level ($|0\rangle$ and $|1\rangle$) and three-level ($|0\rangle$, $|1\rangle$, and $|2\rangle$) diagrams.[2,14] However, in the diagrams that produce the anharmonic oscillations, the first two interactions involve only the $|0\rangle$ and $|1\rangle$ states; there is no branching. In a quantum beat, the first interactions couple the ground and singly excited states of *two different modes*, but the emission occurs from the *singly excited state of a single mode*. In anharmonic oscillations, the first interactions involve ground and singly excited states of *a single mode*, but the emission occurs from both *doubly and singly excited states of the same mode*; the emission arises at the same frequency only because of inhomogeneous broadening. The inhomogeneous broadening makes it possible for the two distinct types of diagrams to be accidentally degenerate.

The ''two-level'' diagrams[2] (i.e., those diagrams that have transitions between only the ground state and a fundamental) have a coherence between the $|0\rangle$ and $|1\rangle$ levels after the first pulse, which corresponds to a density matrix element of $\rho_{01}(\omega)$ that evolves at frequency ω. The system interacts with the second pulse twice; the first interaction takes $\rho_{01}(\omega)$ into either $\rho_{00}(0)$ or $\rho_{11}(0)$ which have no phase evolution,

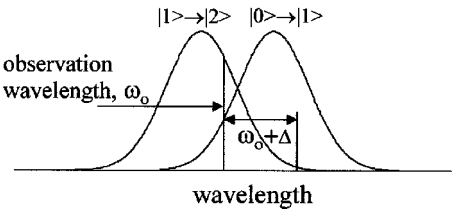

FIG. 3. A schematic illustration of the inhomogeneously broadened envelopes of the 0–1 transition and the anharmonically redshifted 1–2 transition as a function of transition frequency. The vertical lines represent the 0–1 transition frequencies of the two distinct subensembles that contribute to the echo at the noted observation frequency. The anharmonic beats arise because the two-level echo that originates at and is emitted from ω_0 of the 0–1 band, interferes with the three level echo that originates on the blue side of the 0–1 band at $\omega_0+\Delta$ and is emitted from the blue side of the 1–2 band at ω_0.

and the second interaction takes both these elements into the $\rho_{10}(-\omega)$ coherence, which then evolves at frequency $-\omega$ (note the negative frequency that implies rephasing). The phase differences caused by inhomogeneous broadening that occurred in the time τ between the first and second pulse is reversed by time 2τ. Summing ω over all the frequencies in the inhomogeneous line produces a macroscopic polarization that dephases as a free induction decay (FID) after the first interaction and that rephases and dephases again as an FID at a time τ after the second pulse, which generates the echo pulse in the phase-matched direction. The single diagram involving the $|0\rangle$, $|1\rangle$, and $|2\rangle$ levels is responsible for the vibrational echo signal contribution from a 1–2 coherence. The density matrix elements corresponding to this diagram are $\rho_{00}(0)\rightarrow\rho_{01}(\omega)\rightarrow\rho_{11}(0)\rightarrow\rho_{21}(-(\omega-\Delta))$, where Δ is the anharmonic frequency shift of the 1–2 transition relative to the 0–1 transition and $\rightarrow$ represents an interaction with the optical *E* field.

The origin of the observed oscillations in this system lies in the manner in which the multilevel coherences are prepared and evolve in time. The monochromator measures the signal from all oscillators emitting in a narrow bandwidth centered at frequency, ω_0. There are two subensembles of molecules that can emit at ω_0. Figure 3 is useful for understanding the two subensembles. It displays a schematic of the inhomogeneously broadened 0–1 and 1–2 absorption lines. The 1–2 line is displaced to the red (lower energy) by the anharmonic shift. The observation wavelength is on the red side of the 0–1 transition at frequency, ω_0. Another frequency in the 0–1 line at $\omega_0+\Delta$ is marked. Molecules with $\rho_{10}(-\omega_0)$ (third interaction) and the corresponding $\rho_{01}(\omega_0)$ (first interaction) will emit at ω_0 (two level diagrams). Molecules with $\rho_{21}(-\omega_0)$ (third interaction) and the corresponding $\rho_{01}(\omega_0+\Delta)$ (first interaction), will also emit at ω_0 (three level diagram involving the ground state, fundamental and overtone of a single mode). The 1–2 transition frequency of this second set of molecules is at $(\omega_0+\Delta)-\Delta$; that is, their 0–1 transition frequency is $\omega_0+\Delta$, and the 1–2 emission frequency is redshifted by the anharmonic shift, Δ, bringing it to ω_0.

The frequency at which the oscillators emit, ω_0, is the frequency at which the oscillators rephase to form the vibrational echo pulse. In the diagrams involving only the $|0\rangle$ and

$|1\rangle$ levels, the density matrix evolves as $\rho_{00}(0)\rightarrow\rho_{01}(\omega_0)\rightarrow\rho_{00}(0)$ (or $\rho_{11}(0)$)$\rightarrow\rho_{10}(-\omega_0)$. The two level diagrams dephase and rephase at ω_0. In the diagram involving the $|0\rangle$, $|1\rangle$, and $|2\rangle$ levels, the situation is different. For a molecule with 0–1 transition frequency $(\omega_0+\Delta)$, the density matrix evolves as $\rho_{00}(0)\rightarrow\rho_{01}(\omega_0+\Delta)\rightarrow\rho_{11}(0)\rightarrow\rho_{21}(-((\omega_0+\Delta)-\Delta))=\rho_{21}(-\omega_0)$. Thus, the coherence produced by the three level diagram dephases at $(\omega_0+\Delta)$ but rephases at ω_0, producing a polarization at ω_0. At τ, the time of the second pulse, there is a phase difference between $\rho_{01}(\omega_0)$ and $\rho_{01}(\omega_0+\Delta)$ equal to $\Delta\times\tau$. After the second pulse, both oscillators begin rephasing at ω_0. Although the vibrational echo polarizations produced by both types of diagrams have the same frequency, the two polarizations do not have the same phase. As τ is increased, the phase difference advances, giving rise to the oscillations in the ''single frequency'' detected signal. The analysis is identical for a three pulse stimulated vibrational echo. The oscillations can only occur when the first pulse can prepare a 0–1 coherence at both frequencies ω_0 and $\omega_0+\Delta$; if the inhomogeneous linewidth is much smaller than the anharmonicity, then no oscillations will be detected at third order. The mechanism applies whether or not the echo is spectrally resolved. The mechanism does not involve time gating of the interference between two distinct frequencies.[31] The oscillations come from the evolution of the phase relationship of two distinct subensembles of molecules that emit at the same frequency. Unlike a quantum beat, a branching transition is not involved in the first interaction, and unlike a quantum beat, a sufficiently broad inhomogeneous line is required for the oscillation to occur. The inhomogeneous broadening is necessary to permit the emission from the two types of diagrams to be accidentally degenerate. The anharmonic oscillations are one type of accidental degeneracy beats.

In the upper VES in Fig. 2, on the far red sides of the *A* and *S* peaks, are distinct features indicated by the arrows that are split from the 0–1 transition absorption maxima by ~25 cm^{-1}. These features arise from contributions to the vibrational echo signal that involve the combination band transition, that is, a transition that results in both the *A* and *S* states being excited. The frequency of the combination band transition, ω_{AS}, differs from the sum $\omega_A+\omega_S$ by an amount Δ_c, the combination band shift. For $Rh(CO)_2$acac, the shift is to the red, and $\Delta_c=25\,\mathrm{cm}^{-1}$.[28] An example of the pathway of density matrix elements associated with one of the diagrams that would contribute to the combination band peak on the red side of the *A* band is $\rho_{00}(0)\rightarrow\rho_{0S}(\omega_S)\rightarrow\rho_{SS}(0)\rightarrow\rho_{(S+A)S}(\omega_S-\omega_{AS})\rightarrow\rho_{SS}(0)$. The first interaction prepares a coherence between the ground state (00) and $v=1$ level of the *S* vibration. Dephasing occurs at frequency ω_S. The second interaction produces a population in the $v=1$ level of the *S* vibration. The third interaction prepares a coherence between the $v=1$ level of the *S* vibration and the combination band state in which the $v=1$ states of both *A* and *S* are excited. This coherence evolves at frequency $(\omega_S-\omega_{AS})$. $(\omega_S-\omega_{AS})=\omega_S-(\omega_A+\omega_S-\Delta_c)=-(\omega_A-\Delta_c)$. The negative sign indicates that rephasing occurs at frequency $(\omega_A-\Delta_c)$. The final interaction is emission from the combination band state, *AS*, to *S* at frequency $(\omega_{AS}-\omega_S)=(\omega_A+\omega_S-\Delta_c-\omega_S)=\omega_A-\Delta_c$. Thus, the echo signal is observed 25 cm^{-1} to the red of the *A* transition frequency.

The combination band peaks that appear on the red side of the *A* and *S* bands occur because the *A* and *S* modes are anharmonically coupled, that is, their oscillations are not strictly independent. In the ultrafast 2D VES experiment, the combination band is accessed through excited state absorption [i.e., initial interaction at 2082 (2010) cm^{-1}, followed by an interaction at 1985 (2057) cm^{-1}], and appears as two peaks that are both shifted to the red of each fundamental transition by 25 cm^{-1}. The 25 cm^{-1} combination band shift, Δ_c, is a measure of the extent of the coupling. In linear spectroscopy, the combination band absorption peak occurs at $(\omega_A+\omega_S-\Delta_c)$, which is at 4067 cm^{-1}. In the 2D vibrational echo experiment, the combination band is manifested as part of the vibrational echo spectrum at ~2000 cm^{-1}, and because it is accessed by a series of resonant interactions, its intensity is much larger than that seen in a linear absorption spectrum.

The high frequency oscillations (see inset Fig. 2) are found at all wavelengths in the VES spectrum. These oscillations are of particular interest here. For the 0–1 transitions of the *A* and *S* lines, which will be discussed in detail below, the high frequency oscillations are caused by a quantum beat between the *A* and *S* mode frequencies. The center-to-center splitting of the *A* and *S* modes is 72 cm^{-1}. This is the nominal beat frequency for the quantum beats shown in the inset of Fig. 2. For example, for one pair of diagrams that give rise to beats in the 0–1 transitions, the density matrix evolves as $\rho_{00}(0)\rightarrow\rho_{0A}(\omega_A)\rightarrow\rho_{AA}(0)\rightarrow\rho_{A0}(-\omega_A)$ and $\rho_{00}(0)\rightarrow\rho_{0S}(\omega_S)\rightarrow\rho_{00}(0)\rightarrow\rho_{A0}(-\omega_A)$, where the subscripts *A* and *S* stand for the first vibrational excited states of the *A* and *S* modes. The two paths dephase at different frequencies because the first interactions with the radiation field in the two paths involve distinct vibrationally excited states, but the two paths rephase at the same frequency. The difference in the dephasing frequencies produces a beat in the vibrational echo signal at the frequency difference. This is a standard quantum beat that arises from a branching transition. In contrast to the anharmonic accidental degeneracy beats, in the quantum beats: (1) the different frequencies in the first interaction arise from distinct coherences, rather than from different locations in a single inhomogeneously broadened line; (2) the identical frequencies in the third interaction arise from identical coherences, rather than from two distinct transitions with accidental spectrally overlapped coherences.

The high frequency oscillations seen in Fig. 2 in the 0–1 portions of the *A* and *S* bands are standard quantum beats. The high frequency oscillations in the overtone and combination band regions of the *A* and *S* bands are akin to the anharmonic beats discussed above. They are accidental degeneracy beats rather than conventional quantum beats. Accidental degeneracy beats will be discussed in detail subsequently.[32] As an example, consider the beats on the *S* overtone transition (1–2 transition). To have a true quantum beat on the *S* overtone transition, it is necessary to have a pair of pathways (diagrams) one of which begins by preparing a coherence between 0 and 1 of *S* and ends with rephasing in the 1–2 transition of *S*, and another that begins by

preparing a coherence between 0 and 1 of A and ends with rephasing in the 1–2 transition of S. The first pathway is $\rho_{00S}(0)\rightarrow\rho_{01S}(\omega_{01S})\rightarrow\rho_{11S}(0)\rightarrow\rho_{21S}(-\omega_{21S})$. The first interaction and dephasing occur at a frequency in the S 0–1 band, ω_{01S}, where an additional subscript, S, has been added to identify the frequency with the S band. The third interaction and rephasing occur at a frequency in the S 1–2 band, ω_{21S}. $\omega_{21S}=\omega_{01S}-\Delta$, where Δ is the anharmonic shift. To have a true quantum beat at the S/A splitting, it is necessary for the first interaction and dephasing to occur at ω_{01A} and the third interaction and rephasing to occur at ω_{21S}. The second pathway would begin as $\rho_{00A}(0)\rightarrow\rho_{01A}(\omega_{01A})\rightarrow\rho_{11A}(0)$ [or $\rho_{00A}(0)$]. The third interaction would have to prepare the density matrix element, $\rho_{21S}(-\omega_{21S})$, that is, the third interaction would have to take the system from either a population in the A mode's first vibrational level or ground state to an overtone (1–2) coherence in the S mode. Such a transition is not possible through a single interaction with the radiation field. The necessary second pathway does not exist at third order. A true quantum beat cannot occur. However, the pathway $\rho_{00A}(0)\rightarrow\rho_{01A}(\omega_{01A})\rightarrow\rho_{00A}(0)\rightarrow\rho_{10S}(-\omega_{10S})$ does exist. With sufficient inhomogeneous broadening, accidental degeneracy of two subensembles of molecules can make the final rephasing frequencies in the two pathways identical (i.e., $\omega_{10S}=\omega_{21S}$), with the dephasing frequencies ω_{01A} and ω_{01S}. Two subensembles are required to produce the beat. Therefore, the high frequency beats in the overtone portions of the VES are a type of accidental degeneracy beat, not a true quantum beat. A similar argument applies to the combination band peak. Like the anharmonic oscillations, the high frequency beats in the overtone and combination band portions of the VES occur because of inhomogeneous broadening and overlapping transitions.

B. Inhomogeneous broadening

The S and A lines in the absorption spectrum are separated by 72 cm^{-1} (see inset Fig. 2). This splitting would give rise to a quantum beat at $\sim$72 cm^{-1} in the 0–1 portion of the S and A VES bands. However, careful analysis of time slices through the data (see inset Fig. 2) at different wavelengths reveals that the period of the S/A quantum beats is not constant. To determine the beat frequency, the data were fit to the convolution of a Gaussian with an exponential. This function is not intended to be a true description of the data. However, the fit removed much of the overall time dependence and left the high frequency beat as the residual to the fit. The residual oscillation was then fit to $\cos(\omega t+\varphi)$. Table I lists the beat frequencies for a number of observation wavelengths moving progressively to the blue on the blue sides of the S and A lines. On the blue sides of the lines, the signal is produced by the 0–1 transitions of the two modes. As is clear from the table, the beat frequency gradually decreases as the observation wavelength is shortened. These observations are inconsistent with a simple picture in which the beat frequency is determined by the frequency difference between the peaks of the S and A lines. As the wavelength of observation within the inhomogeneous lines is changed, the beat frequency changes. (As discussed below, a shoulder on the red side of the S absorption line complicates the analysis of the data on the blue side of the A line. Therefore, most of the analysis will be devoted to the S line.)

TABLE I. Experimental observation wavelengths and beat frequencies.

Spectral band	Observation wavelength (cm^{-1})	Beat frequency[a] (cm^{-1})
S	2081	71.3
S	2083	70.8
S	2085	70.6
S	2087	70.3
A	2011	70.8
A	2013	70.3
A	2015	69.8
A	2017	69.4

[a]The errors on the beat frequencies are estimated to be $\pm$0.1.

To understand the trend in the beat frequencies as the observation wavelength is varied, it is necessary to consider the nature of the solute–solvent interactions that give rise to the inhomogeneous broadening of the S and A bands. Because the CO stretches in $Rh(CO)_2acac$ are inhomogeneously broadened when dissolved in DBP at 150 K, which wavelength(s) in the A line will be associated with a given wavelength in the S line to produce a quantum beat is not immediately obvious. From the analysis, information is obtained on solute–solvent intermolecular interactions and possible sources of inhomogeneous broadening.

To appreciate the manner in which the correspondence between the A and S lines manifests itself in the experiments, it is useful to briefly review the nature of the vibrational echo signal. The Feynman diagrams that relate to the different quantum pathways are a valuable means of expressing the various contributions to the observed signal, but it is important to recognize that the state of each molecule is really a superposition of all of these quantum pathways. Therefore, a single molecule is actually dephasing at both its natural S and A frequencies. In this context, the response of a molecule depends on its particular S and A homogeneous line frequencies that are located somewhere within the S and A inhomogeneous lines.

Because the monochromator selects a very narrow portion of the inhomogeneous line, only those molecules that emit at a frequency within the monochromator's band pass will be detected. A molecule that emits at a particular S wavelength within the monochromator band pass will be observed regardless of the value of the molecule's corresponding A wavelength. The resulting beat is at the frequency $(\omega_{S^0}-\omega_{A_{S^0}})$, where ω_{S^0} is the S frequency observed by the monochromator and $\omega_{A_{S^0}}$ is the associated A frequency. The monochromator detects the subensemble of molecules that emit at ω_{S^0}, which, in principle, can have a variety of associated A frequencies. The observed signal could contain a range of beat frequencies. The amplitude of a particular beat frequency is determined by the probability of having a molecule emitting at ω_{S^0} with an associated A frequency, $\omega_{A_{S^0}}$. Then, the beat frequency observed by the monochromator at ω_{S^0} is related to the average $\omega_{A_{S^0}}$. The functional form of

the beat is the Fourier transform of the distribution of $(\omega_{S^0} - \omega_{A_{S^0}})$. If the distribution is narrow or a single value, the beat will be long lived.

To address the nature of beat frequency $(\omega_{S^0} - \omega_{A_{S^0}})$ as a function of the observation wavelength ω_{S^0}, we employ a simple model that is sufficiently robust to contain the necessary elements of the problem. The system is considered in terms of the two CO local stretching modes, α and β, which are coupled to the solvent and to each other. The local modes are taken to be harmonic oscillators. The Hamiltonian is

$$\underline{H} = \underline{H}_\alpha + \underline{H}_\beta + \underline{H}_{\alpha S} + \underline{H}_{\beta S} + \underline{H}_{\alpha\beta}. \tag{1}$$

$\underline{H}_\alpha$ and $\underline{H}_\beta$ are harmonic oscillator Hamiltonians. $\underline{H}_{\alpha S}$ and $\underline{H}_{\beta S}$ reflect the coupling of the α and β local modes to the solvent. $\underline{H}_{\alpha\beta}$ couples the two oscillators. The eigenkets of $\underline{H}_\alpha$ and $\underline{H}_\beta$ are the harmonic oscillator eigenkets in the raising and lowering operator representation, $|n_\alpha\rangle$ and $|n_\beta\rangle$, with eigenvalues

$$E_\alpha = \hbar\omega_\alpha(n_\alpha + 1/2), \tag{2a}$$

$$E_\beta = \hbar\omega_\beta(n_\beta + 1/2). \tag{2b}$$

$\underline{H}_{\alpha S}$ and $\underline{H}_{\beta S}$ are not specified explicitly. They are taken to give rise to identical Gaussian distributions of local mode energies centered at frequency ω_0. The range of solvent environments that interact with the local mode oscillators is responsible for the distribution of local mode frequencies.

For simplicity, the coupling term is chosen to be bilinear, that is,

$$\underline{H}_{\alpha\beta} = \gamma \underline{x}_\alpha \underline{x}_\beta, \tag{3}$$

where γ is the coupling constant, and x_j is the position operator given in terms of harmonic oscillator raising and lowering operators as[33]

$$\underline{x}_j = \left(\frac{\hbar\omega_j}{2k_j}\right)^{1/2} (\underline{a}_j + \underline{a}_j^+). \tag{4}$$

k_j is the force constant. For a harmonic oscillator, $\omega = (k/\mu)^{1/2}$, and μ is the reduced mass. In the absence of the coupling term, the eigenkets are the product kets, $|n_\alpha m_\beta\rangle$.

The bilinear coupling term in the Hamiltonian results in an infinite matrix. However, we are only interested in the lowest three eigenvalues, which correspond to the ground state and the A and S excited states. In the uncoupled basis, the lowest energy state is $|00\rangle$. This state is only coupled to the doubly excited state $|11\rangle$ by the term in $\underline{H}_{\alpha\beta}$ with two raising operators. The next lowest energy uncoupled states are $|01\rangle$ and $|10\rangle$. These states are coupled to each other via the terms in $\underline{H}_{\alpha\beta}$ with one raising and one lowering operator. They are also coupled to $|12\rangle$ and $|21\rangle$ by the term with two raising operators. To obtain the splitting between A and S observed experimentally, the off-diagonal matrix elements have a magnitude of $\sim$36 cm^{-1}. The difference in energy between the $|00\rangle$ state and the $|11\rangle$ state is $\sim$4000 cm^{-1}. Therefore, the coupling to $|11\rangle$ will have little effect on the energy of $|00\rangle$. The coupling between $|01\rangle$ and $|10\rangle$ will have a significant effect, since these states are degenerate or close to degenerate. However, the coupling between $|01\rangle$ and $|10\rangle$ and the states $|12\rangle$ and $|21\rangle$ will have little effect, again because the differences in the energies are $\sim$4000 cm^{-1}. Therefore, the state $|00\rangle$ is taken to be uncoupled to other states, and the states $|01\rangle$ and $|10\rangle$ are taken to be coupled only to each other. The importance of the other off-diagonal coupling matrix elements was tested numerically by diagonalizing a 16×16 matrix. The influence on the lowest three eigenvalues of including the off-diagonal matrix elements between states with large energy differences was found to be less than 0.1%; therefore, they can be dropped.[34]

In terms of the basis states that represent the CO stretching local modes, the eigenvalues are

$$E_0 = \tfrac{1}{2}\hbar(\omega_\alpha + \omega_\beta), \tag{5a}$$

$$E_A = \hbar(\omega_\alpha + \omega_\beta) - \frac{\hbar}{2}\delta, \tag{5b}$$

$$E_S = \hbar(\omega_\alpha + \omega_\beta) + \frac{\hbar}{2}\delta, \tag{5c}$$

with

$$\delta = \left[\frac{\gamma^2}{\mu^2\omega_\alpha\omega_\beta} + (\omega_\alpha - \omega_\beta)^2\right]^{1/2}. \tag{6}$$

The transition frequencies from the ground state to the A and S states are $\Omega_A = (E_A - E_0)/\hbar$ and $\Omega_S = (E_S - E_0)/\hbar$, respectively. These are given by

$$\Omega_A = \tfrac{1}{2}(\omega_\alpha + \omega_\beta - \delta), \tag{7a}$$

$$\Omega_S = \tfrac{1}{2}(\omega_\alpha + \omega_\beta + \delta). \tag{7b}$$

With this model, it is possible to consider several different mechanisms that can give rise to inhomogeneous broadening of the absorption bands and the effect each mechanism will have on the quantum beat frequency as a function of observation wavelength.

Three models of inhomogeneous broadening are considered in terms CO local mode energies and coupling. In one, the transition energies in the S and A lines are anticorrelated either because the inhomogeneous broadening arises from variations in the local mode coupling or the local mode energies are anticorrelated. In the other two, the inhomogeneous distribution of local mode energies are either completely correlated or totally uncorrelated.

1. The anticorrelated case

First, consider the anticorrelated case. The anticorrelated case is illustrated in Fig. 4(a). An observation wavelength some number of standard deviations to the blue of center on the S line has associated with it a wavelength on the A line the same number of standard deviations to the red of center. In the DBP solvent, the A/S splitting is 72 cm^{-1}. Measurements of the absorption spectrum of $Rh(CO)_2acac$ in the gas phase yield a gas phase splitting of 64.4 cm^{-1}. (The gas phase A and S peaks are located at 2026.6 cm^{-1} and 2091.0 cm^{-1}, respectively.) Therefore, interaction with the solvent shifts the peaks to the red (lower energy), but it increases the splitting. The simplest manner in which the positions of the transitions in the inhomogeneously broadened S and A lines can be anticorrelated is if the solute–solvent intermolecular interactions act only to change the strength of the coupling

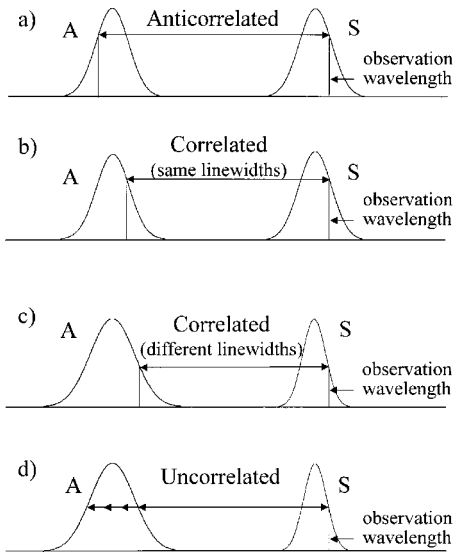

FIG. 4. Diagrams illustrating different possible scenarios that could be involved in the generation of a quantum beat at a single observation wavelength on the *S* line. (a) The frequencies in the *A* and *S* lines are anticorrelated. (b) The inhomogeneous lines have identical linewidths, and the local mode frequencies are correlated. (c) The inhomogeneous lines have different linewidths, and the local mode frequencies are correlated. (d) The inhomogeneous lines have different linewidths, and the local mode frequencies are uncorrelated. Each situation gives rise to a unique prediction for the dependence of the beat frequency on observation wavelength.

between the two local modes. In this case, $\omega_\alpha=\omega_\beta=\omega_0$, that is, the local mode frequencies are independent of the solvent environment. For this situation, the transition frequencies are

$$\Omega_A=\omega_0-\frac{\delta}{2}, \tag{8a}$$

$$\Omega_S=\omega_0+\frac{\delta}{2}, \tag{8b}$$

and

$$\delta=\frac{\gamma}{\mu\omega_0}. \tag{8c}$$

Variations in the coupling parameter, γ, about the average value in the solvent, γ_0, will produce inhomogeneous broadening in which the transition frequencies in the *A* and *S* lines are anticorrelated. For any molecule, as γ increases, the transition frequency in the *A* line moves to the red, and the transition frequency in the *S* line moves to the blue. As the wavelength of observation in the *S* line is moved to the blue, the corresponding transition in the *A* line for the molecules under observation will move to the red. The frequency of the quantum beat, v_b, is

$$v_b=\omega_S-\omega_A. \tag{9}$$

Therefore, as the wavelength of observation moves further to the blue on the *S* line, the beat frequency should increase. This is in contrast to the observed decrease in the beat frequency shown in Table I. Looking at Eq. (7), anticorrelation can also occur if the local mode frequencies are anticorrelated, that is, as ω_α increases ω_β decreases the same amount, and vice versa. (It is difficult to envision a mechanism that would make the local mode frequencies anticorrelated.) The result is basically the same. Anticorrelation would lead to an increase in the beat frequency as the observation wavelength on the *S* band is moved farther to the blue. This is contrary to observation.

2. The correlated case

The local mode frequencies are taken to have a Gaussian distribution with a center frequency ω_0, and a standard deviation σ. Each of the local mode frequencies, ω_α and ω_β, has the same distribution. The probability of having a particular frequency is $P(\omega_i)$, where $P(\omega_i)$ is determined by the position in the Gaussian local mode distribution. The probability of having a particular pair of frequencies is $P(\omega_\alpha,\omega_\beta)=P(\omega_\alpha)\times P(\omega_\beta)$. ω_0 and σ are chosen to reproduce the linear absorption spectrum as closely as possible (see below).

The correlated case is depicted in Figs. 4(b) and 4(c). In terms of the distribution of local mode frequencies, the correlated case arises when $\omega_\alpha=\omega_\beta=\omega$. In this situation, from the model, the transition frequencies are

$$\Omega_A=\omega-\frac{\gamma}{2\mu\omega}, \tag{10a}$$

$$\Omega_S=\omega+\frac{\gamma}{2\mu\omega}. \tag{10b}$$

The absorption spectrum shows that the *A* and *S* lines are close to Gaussian in shape, but they have different inhomogeneous widths. The widths of the *A* and *S* absorption bands are 12.6 cm^{-1} and 10.2 cm^{-1}, respectively, at the experimental temperature, 150 K. (The *S* line develops a shoulder on the red side of the absorption line as the temperature is reduced below room temperature. The analysis given here is restricted to the blue sides of the lines to avoid complications that are caused both by the shoulder and the influences of the overtone and combination bands in the VES.)

First take the *S* and *A* lines to have *identical inhomogeneous widths* [i.e., set $\omega=\omega_0$, a constant in the denominators on the right-hand sides (rhs) of Eqs. 10(a) and 10(b)]. For identical widths [Fig. 4(b)], the correlated case means that for an observation wavelength shifted to the blue of center by a certain energy on the *S* line, the corresponding position on the *A* line is shifted to the blue of center by the identical amount. Moving the detection wavelength farther and farther to the blue on the *S* line results in the corresponding *A* transitions moving identical amounts to the blue. Therefore, the *S*/*A* splitting is independent of the observation wavelength, and the beat frequency will be independent of the observation wavelength. This is contrary to observation. The uncorrelated case, discussed below, has a similar behavior for identical linewidths.

As pointed out above, the *A* and *S* inhomogeneously broadened absorption lines do not have the same widths. The bilinear coupling model yields *A* and *S* linewidths that are not the same, and predicts that the *A* linewidth is wider than the *S* linewidth. The difference in widths arises from the ω in the denominator of the second term on the rhs of Eqs. (10).

TABLE II. Experimental and calculated linewidths. Calculated: local mode distribution $-\omega_0=2045.8\ \mathrm{cm}^{-1}$, $\sigma=6.85\ \mathrm{cm}^{-1}$.

	Symmetric linewidth FWHM (cm^{-1})	Antisymmetric linewidth FWHM (cm^{-1})
Experiment	12.6	10.2
$a=0$ correlated	11.61	11.23
$a=0.0025$ correlated	12.65	10.20
$a=0.0025$ uncorrelated	12.69	10.27

As ω is increased, the second term on the rhs of Eqs. (10), the coupling term, is decreased. Relative to the local mode frequency, the increasing ω in the denominators causes molecules to be shifted less to the blue than they otherwise would be in the *S* line [Eq. 10(b)] and less to the red than they otherwise would be in the *A* line [Eq. 10(a)]. In a corresponding manner, as ω is decreased, molecules are shifted more to the blue in the *S* line and more to the red in the *A* line than they would be otherwise. The result is that the *S* line is narrowed and the *A* line is broadened.

With the *S* line narrower than the *A* line, the correlated case [Fig. 4(c)] no longer predicts that the beat frequency is independent of the observation wavelength. In the calculations, if the *S* line is observed at a particular wavelength on the blue side of the line, there is a single corresponding wavelength on the blue side of the *A* line. However, an observation wavelength some multiple of a standard deviation, $\Delta\sigma_S$, to the blue on the *S* line has associated with it a corresponding wavelength on the *A* line shifted by the same multiple of a standard deviation, $\Delta\sigma_A$. Since σ_A is larger than σ_S, the difference between the *A* wavelength and the *S* wavelength is less than the center-to-center separation of the peaks. Thus, the beat frequency is predicted to be less than the separation of the peaks. As the observation wavelength is moved further to the blue on the *S* line, the separation becomes smaller, and the beat frequency decreases.

Equations (10) predict the qualitatively correct observations. In the linear absorption spectrum the *A* line is wider than the *S* line. In the 2D vibrational echo spectrum, a decreasing beat frequency occurs as the observation wavelength is moved further to the blue on the *S* line. However, the difference in the *A* and *S* absorption linewidths is not large enough, and the change in the beat frequency with observation wavelength is far too small. The closest calculated linewidths are with $\sigma=6.85\ \mathrm{cm}^{-1}$, which yields *A* and *S* linewidths of 11.6 cm^{-1} and 11.2 cm^{-1}, respectively, in contrast to the experimental values of 12.6 cm^{-1} and 10.2 cm^{-1} (see Table II). To reproduce the linear absorption spectrum, it is necessary to increase the strength of the ω dependence in the second term on the rhs of Eqs. (10). In going from the gas phase to the DBP solvent, the transition energies shift to lower energy but the splitting between the *A* and *S* lines increases. In the model Hamiltonian, Eq. (1), there is no term that changes the coupling between the local modes because of interaction with the solvent. A simple heuristic modification of Eq. (6) that has the correct behavior, that is, increases the coupling strength as the frequency moves to lower energy is

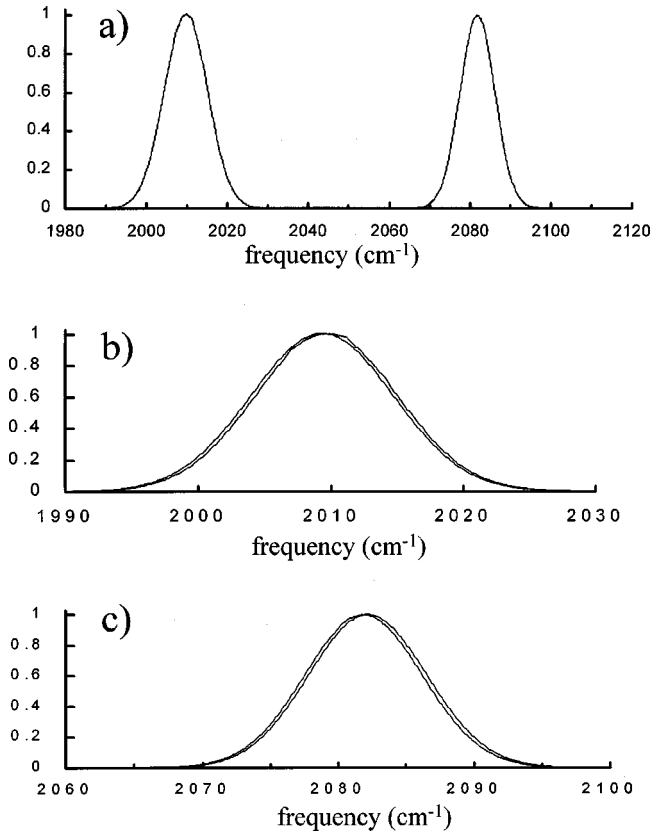

FIG. 5. The linear spectrum predicted by the augmented bilinear coupling model with parameters chosen to mimic the observed linear absorption spectrum of $Rh(CO)_2$acac in DBP. (a) The predicted absorption spectrum assuming complete correlation of the local mode frequencies. The model is able to accurately reproduce the absorption spectrum with the correct peak splitting and linewidths. In parts (b) and (c) the predicted absorption spectrum assuming complete correlation (correlated model) is blown up and overlaid with the predicted spectrum assuming a total lack of correlation (uncorrelated model). The correlated and uncorrelated cases predict essentially identical spectra for the same input parameters.

$$\delta=\left[\frac{\gamma^2}{\mu^2\omega_\alpha e^{a(\omega_\alpha-\omega_0)}\omega_\beta e^{a(\omega_\beta-\omega_0)}}+(\omega_\alpha-\omega_\beta)^2\right]^{1/2}. \tag{11}$$

When $a=0$, the original form of δ is recovered. Using this form, for the correlated case the transition energies become

$$\Omega_A=\omega-\frac{\gamma}{2\mu\omega e^{a(\omega-\omega_0)}}, \tag{12a}$$

$$\Omega_S=\omega+\frac{\gamma}{2\mu\omega e^{a(\omega-\omega_0)}}. \tag{12b}$$

For $\sigma=6.85\ \mathrm{cm}^{-1}$ and $a=0.0025$, the *A* and *S* linewidths are 12.65 cm^{-1} and 10.20 cm^{-1}, respectively, in accord with the experimental values. Figure 5(a), shows the calculated spectrum, and Table II lists the experimental and calculated linewidths. Using Eqs. (12) increases the difference in widths between the *S* and *A* lines, and, therefore, causes the beat frequency to decrease more rapidly as the observation wavelength is moved further to the blue on the *S* line. In fact, the same parameters that reproduce the linear absorption spectrum do a reasonably good job of reproducing the trend in the beat frequency as a function of observation wavelength

TABLE III. (a) Symmetric line–calculated beat frequencies. (b) Antisymmetric line–calculated beat frequencies.

(a)	S line observation freq. cm^{-1}	Anticorrelated beat freq. cm^{-1}	Correlated beat freq. cm^{-1}	Uncorrelated beat freq. cm^{-1}
	2072	52	74.50	70.99
	2077	62	73.25	71.82
	2082	72	72.00	72.60
	2087	82	70.75	73.33
	2092	92	69.50	73.96
(b)	A line observation freq. cm^{-1}	Anticorrelated beat freq. cm^{-1}	Correlated beat freq. cm^{-1}	Uncorrelated beat freq. cm^{-1}
	2000	92	74.00	71.22
	2005	82	73.00	72.00
	2010	72	72.00	72.68
	2015	62	71.00	73.29
	2020	52	70.00	73.88

on the blue side of the S line. Results of the calculations are shown in Table III and discussed further below.

3. The uncorrelated case

The uncorrelated case is depicted in Fig. 4(d). In the uncorrelated case, for a given ω_α value, ω_β can take on a variety of values with the probability for a particular value given by the Gaussian distribution of local mode frequencies. Using the same augmented model that was able to reproduce linear absorption line shapes in the correlated case, the A and S transition frequencies are

$$\Omega_A = \tfrac{1}{2}(\omega_\alpha+\omega_\beta) - \frac{1}{2}\left[\frac{\gamma^2}{\mu^2\omega_\alpha e^{a(\omega_\alpha-\omega_0)}\omega_\beta e^{a(\omega_\beta-\omega_0)}}+(\omega_\alpha-\omega_\beta)^2\right]^{1/2}, \tag{13a}$$

$$\Omega_S = \tfrac{1}{2}(\omega_\alpha+\omega_\beta) + \frac{1}{2}\left[\frac{\gamma^2}{\mu^2\omega_\alpha e^{a(\omega_\alpha-\omega_0)}\omega_\beta e^{a(\omega_\beta-\omega_0)}}+(\omega_\alpha-\omega_\beta)^2\right]^{1/2}. \tag{13b}$$

In contrast to the correlated case, in the uncorrelated case, a range of pairs of local mode frequencies $(\omega_\alpha,\omega_\beta)$ can give rise to a particular transition frequency. In spite of the difference between the correlated and uncorrelated cases, the calculated linear absorption spectrum using the uncorrelated model is virtually identical to the spectrum using the correlated model with the same parameters. Figures 5(b) and 5(c) display the calculated absorption spectra for the A and S lines, respectively, for both the correlated and uncorrelated cases. Table II gives a comparison of the linewidths calculated with the two models using the identical parameters. The uncorrelated widths are slightly larger. A very small change in the parameter a would make them identical. Therefore, the correlated and uncorrelated models cannot be distinguished by comparison of the calculated line shapes with the absorption spectrum.

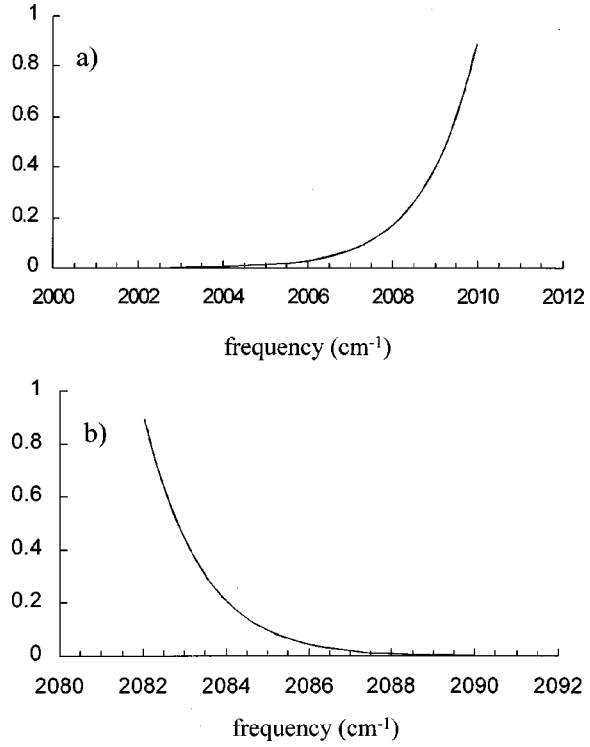

FIG. 6. For a given observation wavelength on the $S(A)$ line the mapping onto the set of transition frequencies on the $A(S)$ line is shown for the case of uncorrelated local mode energies. (a) S line observation wavelength is 2082 cm^{-1}. (b) A line observation wavelength is 2010 cm^{-1}. The curves are the relative probabilities. The calculations show that a single observation wavelength does not map onto a single transition frequency on the other line.

Of particular importance is the fact that a single observation wavelength on the blue side of the S line does not correlate with a single transition frequency in the A line. This is also true for an observation wavelength on the A line. Figure 6 shows the nature of the mapping of a particular observation wavelength on one line to a range of corresponding transition frequencies on the other line. Figure 6(a) shows the mapping from the observation wavelength 2082 cm^{-1}on the S line onto transition frequencies on the A line. Figure 6(b) shows the mapping from the observation wavelength 2010 cm^{-1} on the A line onto transition frequencies on the S line. The figure shows that the mapping is to a broad spread of wavelengths, but the distribution is relatively sharply peaked with a cutoff. Thus, when observing at a particular wavelength on the blue side of the S line, in principle, there will be a spread of beat frequencies rather than a single beat frequency.

The spread in beat frequencies will manifest itself as an oscillation in the data at the average frequency, but the oscillation will be damped as the beat frequencies get out of phase. The nature of the beat was calculated by averaging over the difference between the observation frequency in the S line and the corresponding distribution of transition frequencies in the A line. For each pair ω_α, ω_β that gives rise to the S line observation frequency, the associated beat frequency was weighted by $P(\omega_\alpha,\omega_\beta)=P(\omega_\alpha)\times P(\omega_\beta)$, and the average over beat frequencies was performed for a variety of observation wavelengths. Since there is a spread of

beat frequencies that gives rise to the average, in principle, the damping of the oscillations in the data could be used to extract the spread. However, because the distribution of frequencies in the *A* line that is mapped onto by an observation frequency in the *S* line is relatively sharply peaked, the damping of the oscillations caused by the spread is too slow to be detected given the intrinsic damping caused by homogeneous dephasing of the *S* and *A* transitions.

The results of the calculations of the beat frequencies for the uncorrelated case are given in Table III. As the observation wavelength on the *S* line moves further to the blue, the model predicts that the beat frequency increases, which is contrary to observation. The rate of increase is much slower than for the anticorrelated case.

C. Discussion of the nature of inhomogeneous broadening

Using the coupled local mode model, the nature of solute–solvent interactions that give rise to inhomogeneous broadening was considered in terms of three cases for the correlation between frequencies in the *S* and *A* lines. In one, the transition energies in the *S* and *A* lines are anticorrelated either because the inhomogeneous broadening arises from variations in the local mode coupling constant or the local mode energies are anticorrelated. In the other two, the inhomogeneous distribution of local mode energies are either correlated or uncorrelated. Results of calculations for all three cases are given in parts (a) and (b) of Table III, for the *S* and *A* lines, respectively. The first column in the tables lists the observation wavelengths. The next three columns list the calculated beat frequencies for the three cases. For the uncorrelated case, the beat frequency is the average beat frequency, but as discussed above, the distribution of beat frequencies is narrow.

Consider the blue side of the symmetric line. The experimentally determined beat frequencies are given in Table I. For the anticorrelated case [part (a) of Table III, column 2], as the observation wavelength moves progressively to the blue (higher energy), the beat frequency increases rapidly. For the correlated case [part (a) of Table III column 3], the beat frequency decreases mildly. For the uncorrelated case [part (a) of Table III, column 4], the beat frequency increases mildly. The data are consistent with the correlated case within the context of the calculations using the augmented bilinear coupling theory. Calculations using correlated local mode frequencies are able to reproduce the absorption spectrum as well. The parameters that give the correct linewidths and splitting of the peaks in the absorption spectrum produce the correct trend in the beat frequencies and produce a change in the beat frequency with observation that is similar but not identical to those that are observed. For example, for observation wavelengths 2082 cm^{-1} and 2087 cm^{-1} the correlated case calculations give beat frequencies of 72.00 cm^{-1} and 70.75 cm^{-1}, respectively. The difference is 1.25 cm^{-1}. The experimental values at these wavelengths are 71.1 cm^{-1} and 70.3 cm^{-1}. The difference is 0.8 cm^{-1}. Although the model calculations produce a dependence of the beat frequency with observation wavelength that is ~50% too steep, the correlated case calculations reproduced the correct trend, an accurate description of the absorption line shapes, and come close to quantitatively predicting the beat frequencies.

The anticorrelated case could occur if the solvent produced inhomogeneous broadening by changing the coupling between the local modes. Molecules with large couplings have large *S*/*A* splittings. Such a molecule would be found on the blue side of the *S* line and the red side of the *A* line. Molecules further to the blue on the *S* line would have positions in the *A* line further to the red, giving rise to an increased splitting and a higher beat frequency, as shown in (a) of Table III.

The form of the coupling between the local modes that gives rise to the *A* and *S* modes is an interesting question. The CO stretching transitions are strong. The local mode transition dipole can be calculated[35] from the absorption spectrum.[36] The transition dipole was determined to be $\mu = 0.3$ debye. $Rh(CO)_2$acac is square planar. From the crystal structure,[37] the angle between the CO's is virtually 90° and the center-to-center separation of the CO's is 3.4 Å. Taking the dipole direction to be along the CO bond,[38] the bare transition dipole–transition dipole interaction is 17.2 cm^{-1}. Dividing this value by the DBP dielectric constant of 6.44,[39] gives an interaction of 2.7 cm^{-1}. The *A*/*S* splitting would be twice the interaction. The dielectric constant may not come in as a simple reduction in the magnitude of the bare interaction. However, the fact that the splitting increases when going from vacuum to a dielectric medium and that the splitting is almost insensitive to the solvent[28] suggests that the dominant interaction is not dipole–dipole. Nonetheless, solvent induced variations in the dipole–dipole interaction would result in anticorrelation of the *S*/*A* splitting, which is inconsistent with the beat frequency trend. A possible source of the coupling of the CO local modes to give rise to the *A* and *S* lines is an interaction via the bonding to the Rh, which is discussed below.

The uncorrelated case could occur if the inhomogeneous broadening is dominated by the local solvent structure about the two CO local oscillators. If the solvent structure immediately adjacent to a local oscillator has a major influence on its frequency and if the solvent structure about one CO is distinct and uncorrelated with the solvent structure about the other CO, the local mode frequencies could be uncorrelated. This model is able to reproduce the linear absorption spectrum but not the trend in the beat frequencies.

The observed correlation in the local mode frequencies could arise if macroscopic effects dominate the local mode frequencies. Vibrational frequencies are density dependent.[40] Therefore, variations in local solvent density can affect the local mode frequency. If variations in the density of the glassy solvent occur on a distance scale that is large compared to the size of the $Rh(CO)_2$acac solute, then the CO local modes will experience the same density and have correlated local mode frequencies. This model, while possible, does not seem appropriate. In going from the vacuum to the DBP solid solvent, the absorption peaks shift to the red ~12 cm^{-1}. Variations in the density about the average value are very small compared to the difference between vacuum and the solid. Therefore, such density variations cannot reasonably be expected to produce inhomogeneous linewidths of

$\sim$11 cm^{-1} when the vacuum-to-solid shift is only $\sim$12 cm^{-1}.

The source of the solvent induced distribution of correlated local mode energies may come from the nature of the bonding in metal carbonyls. Gas phase CO has its vibrational transition at $\sim$2130 cm^{-1}. Metal carbonyls have their CO stretching modes shifted to the red on the order of 100 to 200 cm^{-1}. This shift has two sources. In making the metal CO bond, some of the electron density that contributes to the CO triple bond is transferred into the formation of the M–C bond. This reduces the bond order below a triple bond. In addition, there is back bonding from the metal d_π orbitals into the CO antibonding π orbital. This back bonding further weakens the CO bond. The result is the redshift in the CO stretching frequencies of metal carbonyls compared to CO.

The Rhacac portion of $Rh(CO)_2$acac is a planar six member aromatic ring. The Rh is one atom of the six-member ring, and it contributes a d_π orbital to the aromatic π system. DBP has aromatic and nonaromatic portions. Different solvent configurations around the Rhacac ring may influence the Rh contribution to the ring bonding. Changing the extent of d_π contribution to the ring's π system will affect the electron density available for bonding to the COs. Changing the d_π electron density available for back bonding to the COs will change the bond strengths directly and change the CO vibrational frequency. Changes in the Rh electron density available for σ bonding to the COs' carbons indirectly influences the CO bond strength. An increase in the Rh–C bond strength results in a decrease in the CO bond strength, and vice versa. The important point is that even anisotropic interactions of the solvent with the Rhacac ring that produce changes in the Rh electron density available for the $Rh(CO)_2$ bonding will have the identical effect on both COs. Thus, anisotropic interactions with the solvent can give rise to correlated changes in the CO local mode vibrational frequencies.

The proposed mechanism would give rise to correlated local mode frequencies. The distribution of the local mode frequencies produces the inhomogeneous *A* and *S* lines. DBP is a relatively anisotropic molecule that could create a broad distribution of interactions with the $Rh(CO)_2$acac. These interactions generate relatively wide inhomogeneous lines. The $Rh(CO)_2$acac *A* and *S* linewidths in hydrocarbon solvents are considerably narrower than those in DBP.[41] This is consistent with the proposed mechanism.

The correlated local mode frequency model comes closest to reproducing the data. It is the only one of the three scenarios that produces the correct dependence of the beat frequency on the observation wavelength. However, the data dependence on the observation wavelength is not quite as steep as predicted. It is possible that the mechanism responsible for the trend in beat frequencies is not caused solely by the distribution of correlated local mode frequencies. For example, small variations in the transition dipole–transition dipole interaction between the CO oscillators could give rise to a small anticorrelated contribution. In addition, there could be some influence on the local mode frequencies caused by direct uncorrelated local solvent structure variations. Since the anticorrelated and uncorrelated mechanisms result in the opposite trend in the beat frequency with observation wavelength from the correlated mechanism, some contribution from either or both of them would produce a beat frequency dependence that is less steep than predicted by theory.

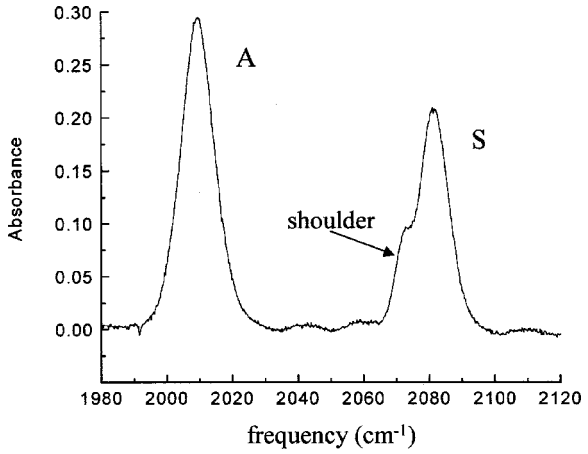

FIG. 7. The experimental linear absorption spectrum of $Rh(CO)_2$acac in dibutylphthalate at 150 K with solvent background subtracted. Note the appearance of the shoulder on the red side of the symmetric peak. This is not present in the room temperature absorption spectrum nor is it present at low temperature when the solvent is PMMA.

Further experimental examination should provide additional insights into the sources of inhomogeneous broadening. As mentioned above, one of the problems with the system studied here is that there is a shoulder on the red side of the *S* absorption line. A detailed spectrum taken at the experimental temperature, 150 K, with the solvent background subtracted is shown in Fig. 7. The *S* peak was fit to the sum of two Gaussians. The shoulder's peak is centered at 2072 cm^{-1}. This shoulder does not occur at room temperature (see inset Fig. 2). The shoulder develops as the sample is cooled and goes away when the sample is warmed up. As the sample is cooled and the shoulder grows in, the area of the total peak is conserved. The spectrum of $Rh(CO)_2$acac in poly(methyl methacrylate) does not have a shoulder at room temperature or at low temperature. It is possible that the shoulder occurs because of a specific association of the solute with the solvent. At low temperature, the benzene moiety of the DBP solvent may form a stable associated structure with the Rhacac six member aromatic ring, producing a well-defined shift in the spectrum. As discussed above, changes in the Rh contribution to the ring bonding can affect the CO frequency.

If such an association is responsible for the shoulder on the *S* line, then there should be a corresponding peak for the *A* line. However, a peak is not visible. Therefore, it must be buried under the *A* line. There is some evidence that this is the case. While the high frequency quantum beats observed on the blue side of the *S* line appear to be composed of a single oscillation (see inset Fig. 2), the beats on the *A* line appear to have a distinct high frequency modulation. The oscillatory component of these data can be fit with two cosine functions in the same manner that the *S* line data was fit with a single cosine function. A Fourier transform of the *A* line data displays a double peak while a Fourier transform of

the *S* line data shows a single peak. The lower frequency component of the two beat frequencies in the *A* line data is $\sim 62\ cm^{-1}$. Then, the *A* line peak corresponding to the *S* line shoulder is located at $\sim 2010\ cm^{-1}$. This wavelength is consistent with the *A* line peak corresponding to the *S* line shoulder being buried under the main *A* line, and it is not independently observable in the linear absorption spectrum. The presence of this buried peak makes the trend in the *A* line beat frequencies with observation wavelength difficult to analyze. As seen in Table I, the trend for the *A* line is the same as that of the *S* line. Future experiments will be conducted in a system that does not display a shoulder, making possible a direct comparison of the *A* line and *S* line beat frequency trends.

IV. CONCLUDING REMARKS

Ultrafast infrared two-dimensional vibrational echo spectroscopy has been used to examine solute–solvent interactions. The symmetric and antisymmetric CO stretching modes of $Rh(CO)_2$acac in dibutylphthalate were studied. The vibrational echo spectrum eliminates the solvent background and displays many features that are not seen in the linear absorption spectrum. The 2D spectrum also provides information that cannot be obtained from the 1D vibrational echo experiment. In the absorption spectrum, there is one peak for each mode. In the VES there are three regions for each mode, the $v=0-1$ transition, the $v=1-2$ transition, and the combination band feature. The decays of the features are related to the solute–solvent dynamics and provide information on pure dephasing and spectral diffusion.[8]

The VES has two modulations, a high frequency modulation and a low frequency modulation. The high frequency modulation of the *S* and *A* 0–1 VES is a quantum beat, which is produced because there is a branching transition. The ground vibrational state is coupled to two excited states, the *S* and *A* states. The beat frequency is determined by the splitting between the *S* and *A* lines. The low frequency modulation is caused by the anharmonicity of each transition. The modulation is at the difference between the 0–1 and 1–2 transition frequencies. This modulation is not a normal quantum beat. It does not involve a branching transition. The anharmonic modulation requires inhomogeneous broadening that is greater than the anharmonic frequency shift. It is an accidental degeneracy beat. The mechanism that gives rise to the anharmonic oscillation was described in some detail.[14] It is different from the previously proposed mechanism.[2,31]

Information on the nature of solute–solvent interactions is contained in the manner in which the quantum beat frequency depends on the wavelength of observation. As the observation wavelength is shifted farther to the blue on the blue side of the *S* line, the beat frequency decreases. A model of the interaction of the local CO oscillators with the solvent was used to investigate the manner in which solute–solvent interactions create inhomogeneous broadening of the *A* and *S* lines. The results indicate that the frequencies of the two CO local oscillators are highly correlated. Such correlation could arise from interactions between the solvent and the six member aromatic Rhacac ring that would cause changes in the Rh–CO bonding. Even anisotropic solvent interactions with the ring would produce correlated changes in the CO local oscillator frequencies by changing the bonding between Rh and the two COs in an identical manner. Additional experimental and theoretical work will be required to enhance understanding of such solute–solvent interactions. Both the experiments and theory presented here should be taken to be preliminary. Nonetheless, they demonstrate that new types of information can be obtained from the application of 2D vibrational echo spectroscopy to molecular systems.

ACKNOWLEDGMENTS

This work was supported by the National Institutes of Health (1RO1-GM61137), the National Science Foundation (DMR-0088942), and AFOSR (F49620-94-1-0141). One of the authors (K.A.M.) is supported in part by an Abbot Laboratories Stanford Graduate Fellowship.

[1] D. Zimdars, A. Tokmakoff, S. Chen, S. R. Greenfield, M. D. Fayer, T. I. Smith, and H. A. Schwettman, Phys. Rev. Lett. **70**, 2718 (1993).
[2] K. D. Rector, A. S. Kwok, C. Ferrante, A. Tokmakoff, C. W. Rella, and M. D. Fayer, J. Chem. Phys. **106**, 10027 (1997).
[3] K. D. Rector, C. W. Rella, A. S. Kwok, J. R. Hill, S. G. Sligar, E. Y. P. Chien, D. D. Dlott, and M. D. Fayer, J. Phys. Chem. B **101**, 1468 (1997).
[4] K. D. Rector and M. D. Fayer, Int. Rev. Phys. Chem. **17**, 261 (1998).
[5] P. Hamm, M. Lim, W. F. Degrado, and R. M. Hochstrasser, J. Chem. Phys. **112**, 1907 (2000).
[6] M. C. Asplund, T. Zanni, and R. M. Hochstrasser, Proc. Natl. Acad. Sci. U.S.A. **97**, 8219 (2000).
[7] K. D. Rector, D. E. Thompson, K. Merchant, and M. D. Fayer, Chem. Phys. Lett. **316**, 122 (2000).
[8] M. A. Berg, K. D. Rector, and M. D. Fayer, J. Chem. Phys. **113**, 3233 (2000).
[9] K. D. Rector, M. Berg, and M. D. Fayer, J. Phys. Chem. **105**, 1081 (2001).
[10] R. B. Williams, R. F. Loring, and M. D. Fayer, J. Phys. Chem. (in press).
[11] G. Bodenhausen, R. Freeman, G. A. Morris, and D. L. Turner, J. Magn. Reson. **31**, 75 (1978).
[12] W. P. deBoeij, M. S. Pshenichnikov, and D. A. Wiersma, Chem. Phys. **1998**, 287 (1998).
[13] S. M. Gallagher, A. W. Albrecht, T. D. Hybl, B. L. Landin, B. Rajaram, and D. M. Jonas, J. Opt. Soc. Am. B **15**, 2338 (1998).
[14] K. A. Merchant, D. E. Thompson, and M. D. Fayer, Phys. Rev. Lett. **86**, 3899 (2001).
[15] S. Mukamel, *Principles of Nonlinear Optical Spectroscopy* (Oxford University Press, New York, 1995).
[16] S. Mukamel, A. Piryatinski, and V. Chernyak, Acc. Chem. Res. **32**, 145 (1999).
[17] K. D. Rector and M. D. Fayer, J. Chem. Phys. **108**, 1794 (1998).
[18] K. D. Rector, A. S. Kwok, C. Ferrante, R. S. Francis, and M. D. Fayer, Chem. Phys. Lett. **276**, 217 (1997).
[19] K. D. Rector, M. D. Fayer, J. R. Engholm, E. Crosson, T. I. Smith, and H. A. Schwettmann, Chem. Phys. Lett. **305**, 51 (1999).
[20] K. D. Rector, D. A. Zimdars, and M. D. Fayer, J. Chem. Phys. **109**, 5455 (1998).
[21] W. M. Zhang, V. Chernyak, and S. Mukamel, J. Chem. Phys. **110**, 5011 (1999).
[22] M. C. Asplund, M. Lim, and R. M. Hochstrasser, Chem. Phys. Lett. **323**, 269 (2000).
[23] O. Golonzka, M. Khalil, N. Demirdoven, and A. Tokmakoff, Phys. Rev. Lett. **86**, 2154 (2001).
[24] M. Khalil, N. Demirdoven, and A. Tokmakoff, Chem. Phys. (in press).
[25] A. Tokmakoff, A. S. Kwok, R. S. Urdahl, R. S. Francis, and M. D. Fayer, Chem. Phys. Lett. **234**, 289 (1995).
[26] D. E. Thompson, K. A. Merchant, and M. D. Fayer, Chem. Phys. Lett. (in press).
[27] D. E. Thompson and J. C. Wright, J. Phys. Chem. A **104**, 11282 (2000).
[28] J. D. Beckerle, M. P. Casassa, R. R. Cavanagh, E. J. Heilweil, and J. C. Stephenson, Chem. Phys. **160**, 487 (1992).

[29] A. I. Lvovsky and S. R. Hartmann, Laser Phys. **6**, 535 (1996).
[30] M. Koch, J. Feldmann, G. von Plessen, E. O. Gobel, P. Thomas, and K. Kohler, Phys. Rev. Lett. **69**, 3631 (1992).
[31] P. Hamm, M. Lim, M. Asplund, and R. M. Hochstrasser, Chem. Phys. Lett. **301**, 167 (1999).
[32] K. A. Merchant, D. E. Thompson, and M. D. Fayer (in preparation).
[33] M. D. Fayer, *Elements of Quantum Mechanics* (Oxford University Press, New York, 2001).
[34] K. K. Lehmann, J. Chem. Phys. **96**, 8117 (1992).
[35] P. F. Bernath (Oxford University Press, 1995), pp. 1–35.
[36] E. J. Heilweil, R. R. Cavanagh, and J. C. Sephenson, J. Chem. Phys. **89**, 230 (1988).
[37] F. Huq and A. C. Skapski, J. Mol. Struct. **4**, 411 (1974).
[38] E. Park, S. Andrews, and S. G. Boxer, J. Phys. Chem. (London) **103**, 9813 (1999).
[39] J. A. Riddick and W. B. Bunger, *Organic Solvents Phycial Properties and Methods of Purification*, 3rd ed. (Wiley-Interscience, New York).
[40] D. J. Myers, M. Shigeiwa, B. J. Cherayil, and M. D. Fayer, J. Phys. Chem. B **104**, 2402 (2000).
[41] T. P. Dougherty, W. T. Grubbs, and E. J. Heilweil, J. Phys. Chem. **98**, 9396 (1994).